



Cite this: *Analyst*, 2021, **146**, 403

Graphene field-effect transistors as bioanalytical sensors: design, operation and performance†

Anouk Béraud,^{a,b} Madline Sauvage,^{a,c} Claudia M. Bazán,^a Monique Tie,^{a,d} Amira Bencherif^{a,e} and Delphine Bouilly  ^{*a,b}

Graphene field-effect transistors (GFETs) are emerging as bioanalytical sensors, in which their responsive electrical conductance is used to perform quantitative analyses of biologically-relevant molecules such as DNA, proteins, ions and small molecules. This review provides a detailed evaluation of reported approaches in the design, operation and performance assessment of GFET biosensors. We first dissect key design elements of these devices, along with most common approaches for their fabrication. We compare possible modes of operation of GFETs as sensors, including transfer curves, output curves and time series as well as their integration in real-time or *a posteriori* protocols. Finally, we review performance metrics reported for the detection and quantification of bioanalytes, and discuss limitations and best practices to optimize the use of GFETs as bioanalytical sensors.

Received 17th August 2020,
Accepted 11th November 2020

DOI: 10.1039/d0an01661f

rsc.li/analyst

^aInstitute for Research in Immunology and Cancer (IRIC), Université de Montréal, Montréal, Canada. E-mail: delphine.bouilly@umontreal.ca

^bDepartment of Physics, Faculty of Arts and Sciences, Université de Montréal, Montréal, Canada

^cProgram of Molecular Biology, Faculty of Medicine, Université de Montréal, Montréal, Canada

^dDepartment of Chemistry, Faculty of Arts and Sciences, Université de Montréal, Montréal, Canada

^eInstitute for Biomedical Engineering, Faculty of Medicine, Université de Montréal, Montréal, Canada

†Electronic supplementary information (ESI) available: Methodology for literature survey and link to database; methodology and tables for analysis of reported LODs. See DOI: 10.1039/d0an01661f

1. Introduction

Bioanalytical sensors, engineered at the interface between physics, chemistry, biology and nanotechnology, are a class of instruments designed for quantitative analyses of biologically-relevant molecules (*e.g.* nucleic acids, proteins, metabolites, drugs, *etc.*). Such biosensors have numerous applications in a variety of areas including biomedicine,^{1–3} environmental monitoring^{4,5} and public health.^{6,7} Analyte detection and transduction into signal can be mediated by different mechanisms, including optical, electrochemical, electrical or mechanical. In the past decades, advances in the field of nanotechnology have catalyzed remarkable innovation in these different subclasses of bioanalytics sensors, especially through the discovery and production of new nanomaterials. For



Anouk Béraud

Anouk Béraud is an M.Sc. student in Physics at Université de Montréal, Canada. She received her B.Sc. degree from Université de Montréal in 2019, with a dual specialization in Physics and Computer Science. Her master research focuses on instrumentation development to probe surface interactions in graphene field-effect transistor biosensors.



Madline Sauvage

Madline Sauvage is a Ph.D. candidate in Molecular Biology at Université de Montréal, Canada. Previously, she completed a B.Sc. degree in Molecular and Cellular Biology in 2017 followed by a M.Sc. degree in Systems Biology in 2018, both at Université de Montréal. In her thesis, she researches new approaches for the detection and suppression of genetic mutations in breast cancer causing resistance to treatment.



example, gold nanoparticles (AuNPs) and inorganic quantum dots (QDs) have been used in the design of ultrasensitive electrochemical⁸ and optical⁹ biosensors. Materials engineering at the nanoscale has enabled artificial nanopores in solid-state membranes (e.g. Si₃N₄ membrane, SiO₂, SiC and Al₂O₃ films) capable of registering the translocation of individual DNA molecules.¹⁰ Nanocarbon materials such as carbon nanotubes (CNTs) and graphene have also stimulated improvements in optical,^{11,12} electrochemical^{13,14} as well as in MEMS/NEMS (micro/nanoelectromechanical systems) bioanalytical sensors.¹⁵

A specific class of nanomaterial-enabled bioanalytical sensors are field-effect transistors (FETs). In FET biosensors, or bioFETs, the interaction with biological analytes is transduced as a change in the electrical conductance of the sensor. The use of FETs for bioanalytical sensing purposes first appeared around 1980, usually adapted from ion-sensitive field-effect transistors (ISFETs) made for pH sensing.¹⁶ For example, Caras and Janata¹⁷ introduced a penicillin-sensitive bioFET assembled by immobilizing specific enzymes on the surface of an ISFET. Early FET sensors were made using traditional semiconductors (e.g. Si) and oxides (e.g. Ta₂O₅ or Al₂O₃), and were often limited in sensitivity due to their low surface-to-bulk ratio. The discovery of low-dimensional semiconductors with extremely high surface-to-bulk ratios prompted the design of various highly-sensitive FET sensors for the detection of ions and molecules.^{18,19} Among these, silicon nanowire FETs (Si-NWFETs) and carbon nanotube FETs (CNTFETs) have both been extensively demonstrated as bioanalytical sensors^{20–22} and even ultimately miniaturized into single-molecule FETs with biomolecules.^{23–25} Despite good sensing performance, the development of 1D-FETs remains hindered today by practical challenges in the synthesis, manipulation and scalable integration of 1D nanomaterials. On the other hand, 2D semiconductor nanomaterials also benefit from extreme surface-to-bulk ratio, but are much more compatible with established microfabrication processes. While a plethora of van der Waals materials have

been discovered in the past few years,^{26,27} graphene is by far the most available and well-studied specimen among them. Since the isolation of individual graphene sheets from graphite by Novoselov and Geim in 2004,²⁸ graphene has received much attention for its exciting mechanical, thermal and optoelectronic properties.²⁹ In particular, graphene was found to exhibit extremely high charge carrier mobility, as well as remarkable sensitivity to electrostatic changes in its near environment,^{30,31} making it a promising material for sensing applications.

In this review, we focus specifically on graphene field-effect transistors (GFETs) as bioanalytical sensor. GFETs have been demonstrated as sensors in physics and chemistry, for instance as photodetectors,³² gas sensors (e.g. NO₂, NH₃, H₂O)^{33,34} or pH sensors.^{35,36} More recently, GFETs have been introduced as biosensors: for instance, Mohanty *et al.*³⁷ reported in 2008 a GFET biosensor able to detect the hybridization between a tethered single strand of DNA and its complementary sequence. Since then, intensive research has been focused on developing GFETs for biomolecular detection. In the bioanalytical field, GFETs have generated interest as ion sensitive field-effect transistors (ISFETs), especially for the detection of toxicology-relevant ions such as heavy metal ions (e.g. Hg²⁺, Pb²⁺).^{38,39} They have also been shown to detect multiple biologically-relevant molecules such as glucose,⁴⁰ various biomarkers for diseases including cancer,^{41,42} DNA sequences with single-nucleotide mismatch specificity,^{43,44} pathogens such as bacteria^{45,46} and viruses,^{47,48} or drugs like opioids⁴⁹ or antibiotics.⁵⁰ GFETs are often described as having key advantages for biosensing applications, including easy operation, fast response,⁵¹ real-time monitoring,^{52–54} high specificity and sensitivity with detection limits down to the femtomolar^{55,56} and sub-femtomolar range,^{57–59} microfluidic integration^{60–62} and multiplexing capability.^{63–65}

In recent years, there has been several reviews discussing the latest research on graphene and its applications as biosensors.^{66–71} However, there is still a lack of a comprehensive review about GFETs focusing on key parameters for asses-



Claudia M. Bazán

Dr Claudia M. Bazán is a research associate at the Institute for Research in Immunology and Cancer (IRIC) from Université de Montréal. She earned a Ph.D. in Chemical sciences in 2012 from the National University of Córdoba, Argentina, after which she was postdoctoral fellow at Université de Montréal. Her current research focuses on the design and biomedical applications of nanocarbon field-effect transistor sensors.



Monique Tie

Dr Monique Tie is a postdoctoral fellow at Université de Montréal, and previously completed a Ph.D. in Chemistry from the University of Toronto in 2018. Her research interests include transport physics and quantum phenomena in self-assembled low-dimensional nanomaterials.



sing their design, operation and performance, which is essential to progress towards the standardization of this technology and its uptake in industrial, commercial and/or clinical applications. Here we present a critical review of these three aspects of bioanalytical GFET sensors. We cover specifically experiments focusing on the detection of proteins, nucleic acids, bacteria, viruses, small molecules such as glucose, antibiotics or drugs, and heavy ions such as lead, mercury or potassium. We did not investigate pH sensors as they represent a whole field of study by themselves.⁷² In the first part of this review, we briefly explain the fundamentals of GFET operation and review reported approaches for the design and fabrication of such devices. In the second part, we discuss and compare the possible modes of operation of GFETs for the detection and quantitation of bioanalytes. Finally, we review the state of performance metrics reported for this technology and discuss limitations and best practices to optimize the design and performance of GFETs as bioanalytical sensors.

2. Design and fabrication

The design of GFET sensors includes four key components: (1) a graphene layer responsible for the transport of electrical current and the transduction of biosensing events, (2) a set of at least three electrodes as required to operate a transistor, (3) a delivery system allowing tested samples to reach the graphene layer, and (4) a layer of biorecognition elements on the graphene surface allowing for the specific capture of targeted analytes. Fig. 1a illustrates a typical layout for these elements. In the following, we review the role and design principles for each of them.

2.1. Graphene material

Graphene is an atomically-thin material made of a two-dimensional hexagonal lattice of carbon atoms. This structure, with each carbon atom sharing three of its four electrons in

covalent bonds with its nearest neighbors (sp^2 bonds), is at the root of the robust mechanical properties of graphene.⁷³ At the same time, the remaining fourth electrons are delocalized over the two-dimensional lattice in a Π orbital responsible for most of the material's optoelectronic properties.⁷⁴ In the context of GFET sensors, we focus on the electrical and electrostatic properties of the material. Graphene is known for its extremely high mobility surpassing that of excellent metals.^{28,75} Being a semi-metal, its electrical conductance is moderately modulated by local electrostatic fields, allowing to operate the material in a field-effect transistor configuration. Because of this moderate ON-OFF modulation, graphene FETs are typically not considered competitive in pure electronics, compared to state-of-the-art 3D semiconductors such as silicon, or even to its 1D counterpart carbon nanotubes. However, their sensitive electrical conductance combined with their extremely high surface-to-bulk ratio provides them with significant advantages for chemical and biochemical sensing.

Graphene can be produced by several different methods before integration in a FET device. First, graphene can be exfoliated from graphite, a material formed of multiple stacked atomic layers of graphene: the process consists in carefully extracting one monoatomic layer from the bulk graphite. Exfoliation can be achieved by various techniques, including chemical exfoliation,⁷⁶ ball milling method,⁷⁷ or more commonly micromechanical exfoliation, often referred as the "scotch-tape method".⁷⁷ The scotch tape method was the first reported to isolate graphene,²⁸ and typically provides the best electrical properties, including the highest mobilities and least density of defects.⁷⁸ However, it is difficult to obtain large-area flakes with exfoliation, which makes this approach less suitable for large-scale fabrication of devices.⁶⁴ Graphene can also be grown by chemical vapor deposition (CVD), most commonly on metallic substrates like Cu or Ni.⁷⁹ In this approach, a hydrocarbon precursor is introduced at high temperature, leading to graphene nucleation on the metal surface. Epitaxial growth on insulating SiC is also possible, in which case gra-



Amira Bencherif

Amira Bencherif is a Ph.D. candidate in Biomedical engineering at Université de Montréal, Canada. She has a bachelor degree in Engineering Sciences from Phelma/Institut Polytechnique de Grenoble in 2014 and a joint master degree in 2016 from Phelma, EPFL and Politecnico Di Torino, in Micro- and Nanotechnologies for Integrated Circuits. Her current research focuses on nanoscale architectures based on graphene field-effect transistors for single-molecule measurements.



Delphine Bouilly

Dr Delphine Bouilly is a faculty member in Physics as well as a principal investigator at the Institute for Research in Immunology and Cancer (IRIC), both at Université de Montréal. She has a Ph.D. degree in Physics from Université de Montréal in 2013 and was a postdoctoral fellow in Chemistry at Columbia University. Her research group is interested in bionanoelectronics, more specifically in the interactions between biological molecules and nanoelectronic circuits, as well as in biomedical applications of nanoelectronic sensors.





Fig. 1 Design elements of a GFET bioanalytical sensor. (a) Typical layout of a GFET sensor, showing a graphene layer functionalized with bio-recognition elements (red) and immersed in a media containing the target analyte (blue). (b) The graphene is connected with source (S) and drain (D) electrodes to generate electrical current along the atomically-thin layer. (c) Example of packaging with electrical connections to the electrodes and a flow cell with inlet/outlet for sample delivery. The gate (G) electrode, which modulates the electrical conductance of graphene, can be assembled in a (d) back-gate, (e) immersed or (f) co-planar configuration.

phene nucleates following sublimation of the Si atoms.⁸⁰ Graphene grown by CVD is often favored in recent works^{57,81} because it is practical to generate large-area graphene layers, making it the best candidate for scalable GFET production. On the other hand, the mobility may be lower than in mechanically exfoliated graphene⁸² and the transfer process following growth (see next section 2.2) can damage the graphene and leave impurities.⁸³ Finally, another form of graphene is reduced graphene oxide (rGO), often used for its low cost and solution-processability.⁸⁴ To produce rGO, a strong oxidation solution is used to separate graphite layers into suspended graphene oxide flakes, which are then chemically reduced back into graphene.⁸⁵ The oxidation/reduction process tends to leave a high density of defects, which typically causes lower mobilities than in other types of graphene.⁸⁶ Independently of the type of graphene used, most GFET sensor studies report working with a single layer of graphene. Some specifically confirm the presence of a single layer with Raman spectroscopy,^{65,83} as single-layer and few-layer graphene can be difficult to distinguish. Others use few-layers graphene,⁸⁷ but single-layer has been reported to enhance the sensing performance.⁸⁷

2.2. Substrate and electrodes

In order to form a GFET device, graphene must be transferred on a planar substrate that provides physical support to the thin nanomaterial as well as to the electrodes and sample delivery system. The substrate, or at least its top layer, is normally made of a dielectric or other insulating material to avoid unwanted electrical connections between the different electrodes placed on its surface. The most popular substrate for GFETs is degenerately-doped Si covered with a layer of SiO₂

dielectric,^{49,56,61,88–90} which is common in the field of electronics and enables the use of the lower layer as a gate electrode (see Fig. 1d). However, SiO₂ surfaces tend to trap charges and impurities, especially during the transfer process.⁶⁶ Other materials are investigated as substrates, for example sapphire on which graphene can be grown directly, leading to enhanced mobilities.⁸³ Research on more flexible and low-cost substrates is ongoing, for example with materials like flexible polyethylene terephthalate,⁴⁸ silk fibroin⁹¹ or paper.⁹²

Multiple techniques are used to place graphene on its operating substrate, depending on the graphene source. Graphene flakes obtained by mechanical exfoliation can be directly transferred on the substrate from the adhesive tape used for extraction, by stamping the tape on the target substrate.⁹³ This straightforward method provides clean, uncontaminated graphene, but is typically incompatible with large-scale FET production. Graphene growth by CVD is done on metal substrates,⁷⁹ then the graphene is transferred onto a dielectric substrate using either wet or dry transfer methods. In wet transfer, graphene is protected on one side with a soft polymer layer, typically polymethylmetacrylate (PMMA), and the metal substrate on the other side is dissolved in an etching solution. The protected graphene is then rinsed and picked up onto the target substrate.⁹⁴ Alternatively, protected graphene can be separated from the metal by electrochemical delamination.^{95,96} Dry transfer techniques include hot pressing and roll-to-roll methods based on thermal release tape (TRT) applied on the graphene.⁹⁴ Pick-up and stamping with PDMS can also be used for dry transfer of graphene.⁹⁷ In the case of rGO, the flakes can be transferred from solution onto the substrate of choice *via* a number of methods, such as drop-casting,⁴³ dip coating⁹⁸ or vacuum filtration on a membrane which is then



For protein detection, the most common strategy is the use of antibodies as probes, due to their high specificity and affinity for their antigen. For instance, GFETs functionalized with antibodies have been used to detect proteins identified as cancer biomarkers: Kim *et al.*⁴¹ immobilized monoclonal antibodies against the prostate specific antigen (PSA) on a GFET biosensor, demonstrating highly sensitive detection of this biomarker of prostate cancer. In a similar way, monoclonal antibodies on GFETs were used to detect alpha-fetoprotein (AFP), a biomarker of hepatocellular carcinoma (HCC), in patient plasma.¹¹⁵ Other studies have used GFETs with antibody probes for biomarkers to other conditions, such as human Chorionic Gonadotrophin (hCG), a common pregnancy indicator.⁸⁹ Antibodies on GFETs have also been shown to detect surface proteins of bacteria^{46,84,90} or viruses.^{47,48,136,137} For example, Chang *et al.*⁸⁴ and Thakur *et al.*⁴⁶ used anti-*E. coli* antibodies in order to detect the bacteria, and more recently Ono *et al.*⁹⁰ used immunoglobulin G (IgG) to immobilize the gastric pathogen *H. pylori* on GFETs. Similarly, Liu *et al.*⁴⁷ used specific antibodies to achieve rotavirus detection. Recently, GFETs with antibodies were also used to detect the SARS-CoV-2 virus responsible for COVID-19.¹³⁶ Antibody probes were also used for the detection of larger complexes such as exosomes⁴² as well as small molecules such as the pesticide chlorpyrifos.⁵⁶

Aptamers are another type of probe molecules used in GFETs; these are folded single-stranded DNA or RNA oligonucleotides that can bind a target protein or small molecule with high affinity and specificity. Saltzgaber *et al.*⁶⁴ functionalized graphene with aptamers designed to bind specifically to human thrombin proteins. Farid *et al.*¹⁰² reported a GFET functionalized with aptamers for detection of the cytokine interferon-gamma (IFN-gamma) associated with tuberculosis susceptibility. Recently, Wang *et al.*⁶¹ studied the binding kinetics of human immunoglobulin E (IgE) to its specific aptamer, allowing the determination of thermodynamic properties of their interaction. In addition, the use of RNA aptamers has been reported for the detection of small molecules, such as the antibiotic tobramycin.⁵⁰

2.4.2. Strategies for probe immobilization. By far the most popular approach to immobilize probe molecules is through graphene functionalization with the linker molecule 1-pyrenebutanoic acid succinimidyl ester (PBASE).^{42–44,48,53,57,61,64,65,81,83,88,90,115,125} On one end, this molecule contains an aromatic pyrene group that binds to the graphene surface through non-covalent π - π interactions. The other end is made of a succinimidyl ester group, which is prone to form a covalent bond with amine groups *via* nucleophilic substitution.¹³⁸ Probes made of DNA are often immobilized with PBASE, usually *via* an amine-terminated modifier attached at the 3' or 5' extremity of the strand. This approach has been reported for simple ssDNA probes,^{53,65,83,139} and also for more complex ssDNA probes,^{43,125} hairpin-ssDNA probes⁵⁷ and dsDNA probes based on strand displacement,⁴⁴ as described in the previous section. Aptamers can also be immobilized with the same approach.^{61,64} It should be noted that Kim *et al.*¹⁰⁸ reported the immobilization of ssDNA

without terminal modifier *via* covalent coupling of the PBASE directly with the amine of nucleobases (adenine, cytosine, and guanine), and of dsDNA *via* non-covalent interactions between the phosphate groups in the DNA backbone and the succinimidyl ester moiety of PBASE. Instead of directly using PBASE, graphene can be functionalized with 1-pyrenebutyric acid, which is then activated using EDC/NHS chemistry into an NHS-ester.¹⁴⁰ In a different approach leading to the same construct, the pyrene moiety is sometimes directly functionalized to the ssDNA as a modifier to the 3' or 5' termination, and the pyrene-DNA complex is then linked to the graphene; this approach was used in Farid *et al.*¹⁰² to immobilize aptamer probes, and in Fu *et al.*¹²⁹ to immobilize ssDNA probe.

The PBASE approach is also frequently used to immobilize proteins, by covalently reacting the succinimidyl ester group with the amine-terminated residue of an amino acid (*e.g.* lysine) available at the surface of the protein. For instance, this approach was successfully applied to immobilize various antibodies^{90,115} as well as the dCas9 enzyme used for detection in genomic DNA in Hajian *et al.*⁵⁵ Some groups use biotin-streptavidin as an intermediary to immobilize protein probes:^{63,90} for example in Ono *et al.*,⁹⁰ amine sites on the urease probes are functionalized with biotin linkers which are then coupled to streptavidin molecules immobilized on graphene with PBASE. A common aspect of these approaches with proteins is that there are frequently multiple available amine sites on a protein, and thus targeting these provides little control on the orientation of the probe on the sensor surface. This distribution can actually be an advantage for sensing by positioning part of the target-binding sites closer to the graphene surface below the screening limit (see section 4.1).¹⁴¹

Graphene can also be functionalized with covalent moieties, which can then be conjugated with biomolecules. A common reaction to do so is through the use of aryldiazonium salts, in which highly reactive radicals formed from reduced diazonium can directly bind to the carbon lattice of graphene.¹⁴² The functionality of the aryl group is chosen for further bioconjugation with biomolecule probes: for instance, 4-carboxybenzenediazonium tetrafluoroborate (CBDT) creates stable carboxyphenyl anchor groups on the graphene surface. These -COOH moieties can then be activated using EDC-NHS chemistry into a stabilized NHS-ester ready for coupling to an amine group on the probe, as described with PBASE above. Lerner *et al.*⁴⁹ used this approach based on CBDT covalent functionalization followed by EDC-NHS reaction to immobilize an opioid receptor protein for naltrexone detection. Others have reported using the EDC-NHS reaction directly on carboxylated defects spontaneously present on the graphene material.¹¹⁷ In a reverse configuration, the functionalization of graphene with primary amines (-NH₂) was shown using electron beam-generated plasmas produced in Ar/NH₃; amine-terminated ssDNA were coupled with the amine-functionalized graphene using glutaraldehyde as a bifunctional linker.¹⁴³

Covalent and non-covalent immobilization approaches have different impacts on GFET sensors. Covalent functionalization causes a significant structural change in graphene: it trans-





Fig. 2 Transfer curves in GFET bioanalytical sensors. (a) Typical transfer curve I_{ds} (V_g) of a GFET, illustrating key metrics in its use as a sensor: (b) change in the voltage of the charge neutrality point V_{CNP} , (c) change in the transconductance of electrons $g_{m(e)}$ or holes $g_{m(h)}$, and (d) change in the current amplitude, including at the charge neutrality point I_{CNP} . (e) Left: GFET experiment showing a lateral shift of the transfer curve upon exposure to increasing concentrations of its target analyte, here potassium cations. Right: Corresponding shift of V_{CNP} as a function of K^+ concentration. Reprinted with permission from Fakih *et al.*¹¹⁹ © 2019 Elsevier B.V. (f) Left: Experiment with a GFET sensor for *E. coli*, showing a change of transconductance in the p-branch of the transfer curve upon increasing bacteria concentration. Right: Corresponding relative conductance change at fixed bias for different surface functionalization of the sensor. Adapted with permission from Chen *et al.*⁷⁸ © 2014 American Chemical Society. (g) Left: GFET experiment for detecting interferon-gamma protein (IFN- γ), showing a change in all three metrics with exposure to the protein. Right: Response of V_{CNP} and I_{CNP} as function of IFN- γ concentration. Reprinted with permission from Farid *et al.*¹⁰² © 2015 Elsevier B.V.

where V_{CNP} is the gate voltage at the charge neutrality point. The slope g_m is called the transconductance

$$g_m = \frac{W}{L} \mu C_g V_{ds} \quad (2)$$

which depends on the width W and length L of the graphene, μ the mobility of charge carriers and C_g the gate capacitance.¹⁴⁸ Transconductances for holes and electrons are not necessarily the same, in which case the transfer curve is asymmetrical.

Transfer curves can be obtained using any of the three gate electrode configurations described in section 2.2 and illustrated in Fig. 1. The gate capacitance – and thus the transconductance – is highly dependent on this layout. In a back-gate configuration, the gate capacitance is dominated by that of the insulating layer separating graphene from the planar gate electrode, typically an oxide with a thickness t ranging from ~ 10 nm to a few μm . The capacitance of this insulating layer is inversely proportional to its thickness: $C_g \approx C_{ox} = \epsilon_{ox}/t$, with ϵ_{ox} the electric permeability of the dielectric. In the case of immersed or co-planar gate configurations, the shape and position of the gate electrode can vary considerably, but the capacitance is mostly determined by the electrical double layer (EDL) formed at the graphene surface by the reorganization of ions in the electrolyte media. This EDL acts similarly as a very thin dielectric layer – in the range of angstroms to a few nanometers.¹⁴⁹ The resulting gate capacitance is much larger than that of back-gate dielectrics, and can reach levels comparable

to the quantum capacitance C_Q .¹⁵⁰ The gate capacitance is then determined by combining the quantum and EDL capacitances in series: $C_g = [C_Q^{-1} + C_{EDL}^{-1}]^{-1}$.⁶⁶ Gate potentials applied across the EDL can be over two orders of magnitude more efficient than through the back gate: consequently, the sweeping range of gate voltage required to capture the linear p- and n-branches is much smaller for immersed or coplanar gates, typically in the order of ± 1 V,¹⁵⁰ compared to ± 10 V for thin oxides, going up to ± 100 V for thick insulators in the back-gate. In electrolyte media, the range of gate bias sweep must also be restricted to avoid unwanted hydrolysis reactions and other electrochemically-driven reactions at the electrodes.⁶⁶

The choice of gate configuration for a GFET sensor depends on the application. The capture of biomolecular analytes (nucleic acids and proteins) normally occurs during immersion of the probe-functionalized graphene layer in the sample, either an analyte-enriched buffer or a biological sample, such as biomedical (blood, serum, urine, *etc.*), food or environmental. Analyte detection by electrical measurements, though, can occur directly in the same media or after its removal. Immersed or co-planar gate configurations allow electrical measurements directly in electrolytic samples, and are thus usually favored in GFET bioanalytical experiments. The back-gate configuration is generally not used when the GFET interface is immersed with electrolytes, because screening by the EDL can lessen the back-gate voltage. Back-gated GFET sensors are more frequently used for the detection of volatile analytes in gaseous media, for example in applications such as



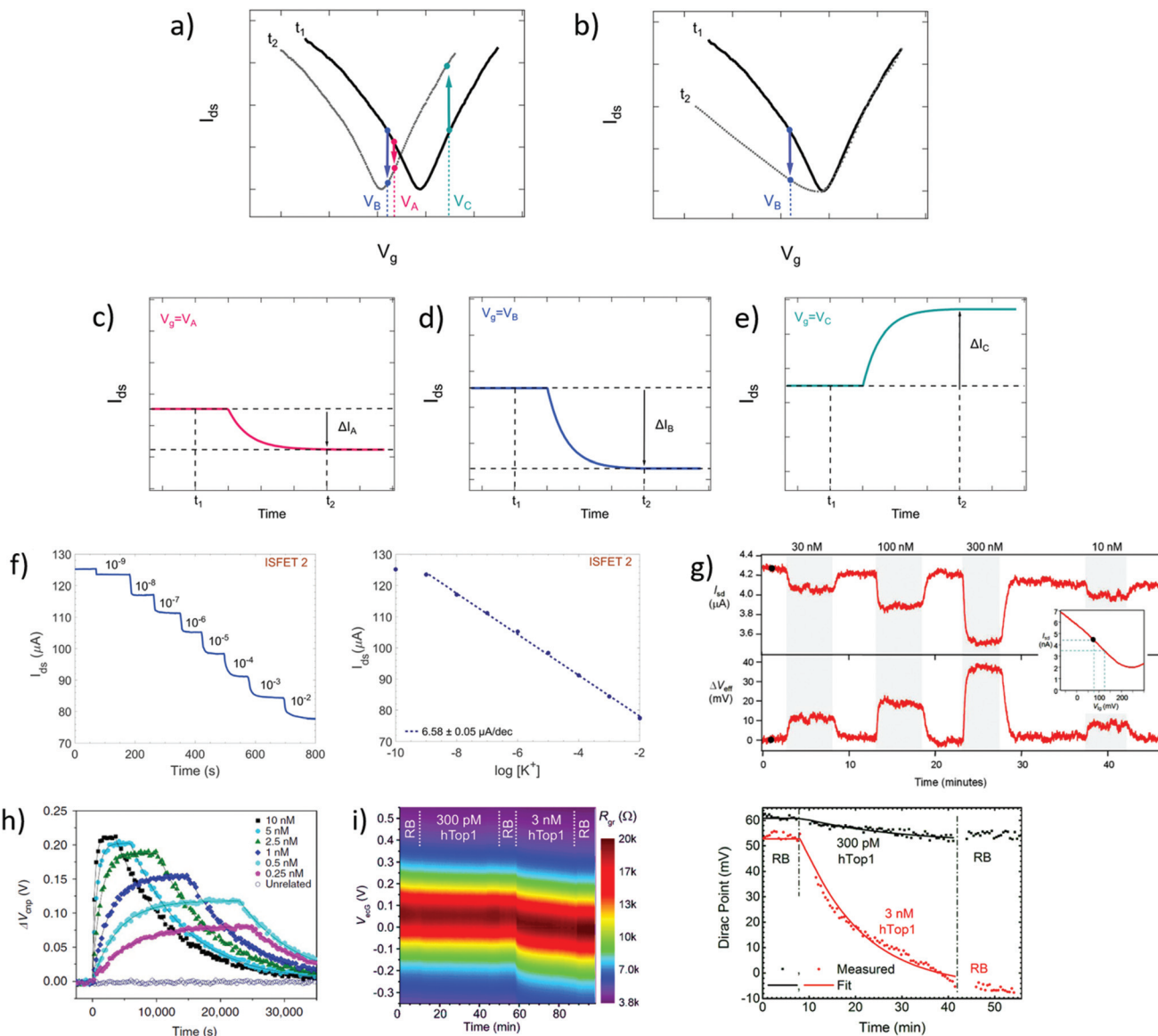


Fig. 4 Time series in GFET biosensors. (a) GFET sensor detecting a left-shift of the CNP voltage, captured in two transfer curves at time points t_1 and t_2 . (b) Same for a system undergoing a change in p-branch transconductance. (c)–(e) Corresponding time series of current $I(t)$ at specific gate voltages V_A , V_B and V_C . (f) Left: Time series of current in a GFET sensor for K^+ ions, recording the exposure to increasing concentrations of analyte. Right: Corresponding change in current as function of K^+ concentration. Reprinted with permission from Fakhri *et al.*¹¹⁹ © 2019 Elsevier B.V. (g) Time series of a GFET sensor for thrombin, recording the introduction of various concentration of analyte separated by washing cycles. Top series shows the current as a function of time, and bottom series the corresponding change in CNP voltage using the conversion described in the inset. Reprinted with permission from Saltzgeber *et al.*⁶⁴ © 2013 IOP Publishing, Ltd. (h) Time series of the change in CNP voltage, also obtained by conversion, showing hybridization and dissociation kinetics between ssDNA probes immobilized on a GFET and different concentrations of the complementary ssDNA. Reprinted with permission from Xu *et al.*⁵³ © 2017 Springer Nature. (i) Left: Two-dimensional time series showing electrical current as a function of both gate voltage and time, here for a GFET sensor targeting the hTop1 enzyme. Right: Time series of the CNP voltage, extracted from the 2D plot, during introduction of hTop1 at two concentrations (right). Reprinted with permission from Zuccaro *et al.*⁵⁴ © 2015 American Chemical Society.

(Fig. 4h). In this approach, the current change ΔI_{ds} is converted to a voltage change with the relation $\Delta V_{CNP} = \Delta I_{ds}/g_m$. It's important to note that this approach is only valid if the transconductance remains constant before and after the addition of targets. As previously mentioned, transfer curves should be provided to confirm that doping is the only mecha-

nism at play. Signal in time series is sometimes normalized as a relative change from a baseline current. Use of normalization can help in assessing signal strength despite sensor-to-sensor variations and effects associated to the medium.⁵⁵ For example, Chen *et al.*⁵⁰ used a simple normalization I_{ds}/I_0 with I_0 the initial current in deionized water and Liu *et al.*⁴⁷ showed



a relative current $(I_{\text{ds}} - I_0)/I_0$ with I_0 the stabilized current after immobilization of the probe molecules. When normalized signal is presented, the conditions used for the baseline should be specified and it is good practice to make available the original time series of the baseline and of the experiment before normalization.

It is possible to avoid the limitations of time series following a constant gate voltage, by implementing a more sophisticated acquisition protocol based on an oscillating gate voltage. In this approach, the gate voltage is continuously swept back and forth over a defined range while the drain–source current is recorded. This results in a two-dimensional mapping of the electrical current as a function of both gate voltage and time. Ideally, the range of the gate voltage sweep is chosen to cover the CNP, which allows to follow the doping state of the graphene at each time point. For example, Zuccaro *et al.*⁵⁴ applied this approach of continuous gate sweeps to produce 2D maps of the low-bias resistance as a function of gate voltage and time, as shown in Fig. 4i (left). This approach allows to extract a time series of the V_{CNP} , as illustrated in Fig. 4i (right), which is a powerful way to quantify the kinetics of the change in doping state.

3.4. Comparison of electrical metrics in “before–after” vs. “real-time” protocols

An important consideration when designing a biosensing experiment with GFET sensors is deciding which type of electrical measurements and metrics to use, and in which sequence to collect them. The design of the acquisition protocol depends on the nature of the scientific question or application for which the biosensor is used. We can divide protocols into two categories: “before–after” and “real-time”. The former refers to experiments comparing the value of a metric, at a specific time point after exposure to the sample, to its baseline value before exposure. This is suitable if the goal is to assess the presence of a target (yes/no type of result). It is also relevant for applications requiring quantification of an analyte: the amplitude of the change in the chosen metric is then compared to a previous calibration of the sensor. However if the application or the scientific question requires information about the kinetics of the biochemical interaction, then a “real-time” protocol recording the evolution of a metric over a relevant period of time is necessary. Among the previously described metrics, some focus on the state of the system at a specific time point, while others allow to monitor the evolution of the system, which makes them naturally more or less convenient for each protocol type.

Transfer curves are especially suitable for before–after measurements, as they provide an informative picture of the electronic state of the sensor at a fixed point in time. Indeed, this type of curve provides information on the doping level, through the CNP position, as well as on both carrier mobilities (electrons and holes), through the transconductance of each branch. Transfer curves can be used to assess completion of different steps of sensor assembly, functionalization and biochemical interactions, by collecting a gate sweep after

each step and comparing the resulting electrical metrics to the initial curve. Even in experiments focused on real-time measurements for reaction kinetics, it is recommended to collect at least initial transfer curves to assess the performance of the sensors, as done by Cohen-Karni *et al.*¹⁷³ In general, before–after analysis of transfer curves is useful for events that have clear before and after states, which are typically before exposure to a reagent and after the reaction with this reagent is considered completed. This type of measurements is commonly used to verify the impact of a passivation layer,⁴⁶ to confirm the presence of functionalization adducts,⁵⁷ to assess the linking of the probes¹²¹ or the linking of the target to the probes.⁴⁴ In sensing experiments, this method is most frequently used for quantitation with various types of analytes including ions,^{121,122,158} proteins,^{102,130} glucose^{40,159} and DNA.^{63,65,83} It is also used for simple yes/no detection, like to assess the presence of a single-mismatched DNA^{43,44,57} or a specific ion.¹⁵⁸ Output curves can be used in the same way as transfer curves in before–after detection schemes, such as in Huang *et al.*,⁴⁵ but they provide less information on the electrostatic state of the graphene and on physical mechanisms occurring in the system (*e.g.* change in doping or diffusion). The analysis of transfer or output curves usually requires post-processing, because the extraction of the CNP voltage, transconductances or output conductance can be performed only after completion of the relevant voltage sweep. From the transfer curve, the CNP voltage is often estimated using the point of the transfer curve with the minimum of current.¹³³ Other studies use curve-fitting to extract the voltage associated with the minimum, usually with a quadratic function⁶³ or with more sophisticated models.⁶⁵ Curve fitting is a more precise method since it is not limited by the width of the gate voltage steps during the measurement. The postprocessing required to determine the transconductance of each branch (g_{h} and g_{e}) involves subjectivity in determining the lower and upper limits of the linear range, which can be considered a limitation of this method. Real-time measurements are usually performed *via* unidimensional or bidimensional time series as described in section 3.3. Real-time measurements are of course essential to study the kinetics of a dynamical reaction.^{40,53–55,88,174} In such experiments, like the study of DNA hybridization by Xu *et al.*⁵³ illustrated in Fig. 4h, the electrical current is monitored during the introduction of analytes and during washing steps. Time series covering washing steps enable to monitor either the removal of non-specific species and unbound analytes or, in the case of weak probes: target affinities, to observe the dissociation of the analyte from the sensor. Time series can be adjusted with a Langmuir binding kinetics model or similar model to estimate adsorption and dissociation constants.^{53,108} Time-resolved measurements can also be used for quantification purposes. For example, Fakhri *et al.*¹¹⁹ studied the influence of K^+ concentration with both transfer curves (Fig. 2e) and time series (Fig. 4f), and observed similar correlations with analyte concentration. This type of experiment is especially conclusive when the signal reaches a clean plateau during target



such as antibodies for protein detection can be upwards of 10 nm in size. To circumvent this issue, some groups have opted to use solutions with low ionic concentration in order to achieve λ_D above 10 nm.^{41,64,181} Others have designed smaller probe molecules such as antibody fragments^{88,182} or aptamers,^{61,146,183,184} allowing to reduce probe length from 10–15 nm to <5 nm, in order to improve device sensitivity. For instance, Kim *et al.*¹⁴⁶ found that replacing a typical antibody probe (~10 nm) with an aptamer probe (~4 nm) on otherwise similar GFET sensors improved sensitivity to the target protective antigen (PA) by 1000 times (12 aM to 12 fM) in 10 μ M PBS ($\lambda_D \sim 23.6$ nm). They also found that signal of PA binding was completely screened out in 1 mM PBS ($\lambda_D \sim 2.3$ nm), even using small aptamer probes, whereas using 10 μ M and 100 μ M PBS (7.3 nm and 23.6 nm, respectively) showed similar signal intensity (determined by the shift in the charge neutrality point) and limit of detection (smallest concentration detected). Interestingly, the range of PA concentration covered before reaching signal saturation was narrower in 100 μ M PBS, indicating lower salt concentration solutions to yield a wider range of detection.

In the case of DNA hybridization experiments, however, many groups have reported detection at very high salt concentrations^{43,81,104} and even for very long DNA sequences.⁴⁴ This reduced limitation to the screening length is likely enabled by the capture of charges close to the FET surface by the first nucleotides of the probe DNA, regardless of its total length. Although high salt concentrations are preferred for stabilizing double-strand DNA, signal and sensitivity can still be improved by decreasing salt concentrations.^{44,53,63,104} Additionally, single nucleotide polymorphism have been detected,^{43,53,81,125} even if located further along the DNA strand than the Debye length. This is explained by the decreased hybridization stability of single mismatched DNA,^{43,81} leading to partial or complete dissociation of the duplex near the graphene surface.

Many strategies for overcoming Debye length limitations while maintaining physiological environmental conditions have been proposed: such as displacing the screening range away from graphene by covering it with a polymer layer permeable to biomolecules¹⁸⁵ or with charged macromolecules to create a fixed-ion region.^{55,186} Similarly, Chen *et al.* reported extending the screening length by adding an MoS₂ layer on graphene.¹⁶² Other strategies include indirect detection of a target *via* the products of its reaction on an enzyme, produced outside of the screening length and diffused to the surface of the GFET⁹⁰ and using a solution containing 12.5 mM of MgCl₂ in a 30 mM Tris buffer, known to provide similar dsDNA stability as in 1 \times PBS, to increase λ_D to 1.6 nm.⁴⁴ Finally, issues related to electrolyte screening can be circumvented all together using a backgate and measuring in air conditions.⁸⁹

4.2. Limit of detection and sensitivity

The performance of GFETs as biological transducers is commonly referred to as their sensitivity.^{43,56,125} Formally, analytical sensitivity describes the ability of the sensor to distinguish

between small differences of analyte concentration.¹⁸⁷ Interestingly, this property is actually rarely assessed in bioanalytical GFET studies; rather, the most widely reported performance metric is the limit of detection (LOD),^{41,48,58,81} which indicates the lowest concentration at which an analyte can be confidently detected by the sensor. Both of these metrics, sensitivity and LOD, are often conflated, yet they represent distinct standards.

Sensitivity is a crucial performance metric for quantitation applications, in particular when it's required to identify analyte concentration with great precision. Sensitivity can be assessed from the calibration curve of the sensor, *i.e.* the evolution of a chosen electrical metric (ex. CNP voltage, current, see section 3) as function of analyte concentration, as illustrated in Fig. 5a. Sensitivity is generally quantified as the slope S of the linear regime of the curve, given by

$$S = \frac{\Delta X}{\Delta N}, \quad (4)$$

where ΔX is the variation of the electrical metric corresponding to a change ΔN in analyte concentration. As discussed in section 3, analyte–sensor interactions in GFETs are often transduced as a change in CNP voltage, yet the exact relation between ΔV_{CNP} and analyte concentration is complex and depends on the precise layout of the functionalized graphene interface and of its coupling to analyte and media. Sensitivity can however be assessed empirically. This is straightforward when the CNP voltage is directly measured as the metric, for instance in before–after experiments with transfer curves: Fakhri *et al.*¹¹⁹ used this approach to assess the sensitivity of their ion sensor in mV per decade. Most often, the measured electrical metric is the drain–source current, especially in real-time experiments, in which case the sensitivity should also be proportional to the transconductance g_m (per eqn (1)). This explains why conventionally, the gate voltage for time series is chosen at the place in the curve with the highest transconductance value.^{64,129} Transconductance itself is proportional to the mobility μ of the graphene, the gate capacitance C_g and the width-to-length ratio W/L of the graphene surface (eqn (2)). In addition, it is generally understood that the sensitivity of a GFET is also limited by noise:¹⁸⁸ the larger the variance in the signal, and thus in the calibration curve, the more difficult it is to distinguish between close concentrations of analyte. Along this line, Fakhri *et al.*³⁵ argue that maximizing material mobility, sensor active area and capacitive coupling allows to minimize noise and improve sensitivity. In general however, the sensitivity of GFETs as biosensors has not been extensively studied or reported. A deeper understanding of its underlying factors and of their relative importance would be valuable to better design GFETs, especially for applications requiring precise quantitation of the analyte.

The limit of detection is a different important performance metric, that determines the minimal concentration of analyte detectable by the sensor. The LOD is determined as the concentration at which signal exceeds the baseline by an interval of confidence, as illustrated in Fig. 5a. A low LOD depends





Fig. 5 Sensitivity and limit of detection (LOD) in GFET biosensors. (a) Typical calibration curve for a GFET sensor, showing the change in a given electrical metric as a function of analyte concentration. Sensitivity represents the slope of the linear regime, while the LOD is the concentration at which the change in the metric exceeds a chosen confidence interval. (b–c) Methods for the experimental determination of the LOD based on extrapolation and direct measurement, respectively. (d) LODs reported in the literature for GFETs, classified by analyte type: ions, small molecules, DNA and proteins. Data points are also separated as function of the type of graphene used in GFET fabrication (ME = mechanical exfoliation, CVD = chemical vapor deposition, rGO = reduced graphene oxide). (e) Reported LODs for DNA detection represented as function of the length of the targeted DNA sequence.

positively on signal strength and is limited by noise and other sources of variance in the measurements. Although distinct, the LOD and sensitivity can be correlated. For instance, in Fig. 5a, we can see that improving the sensitivity or the slope in the calibration curve is likely to lower the LOD. The LOD is relevant for detection and also for quantitation of analytes: it determines the lower bound of the dynamic range of the sensor, the upper end being limited by the saturation of the signal. In practice, the required LOD depends on the purpose of the sensor: for some applications, a predefined LOD needs to be achieved as prescribed by norms or regulations, for example safe Pb^{2+} levels in children's blood¹²¹ or glucose levels associated with diabetes.¹⁵⁹ In the development of GFET biosensors, the LOD is the most frequently reported indicator of performance, and is often benchmarked against other detection techniques, such as PCR-based techniques for DNA detection,⁸¹ or ELISA tests for immunoassays.¹⁷⁴ We surveyed the literature on GFETs used as bioanalytical sensors and retrieved 61 studies reporting a value for the LOD (see the ESI† for a list of the studies). An interesting observation from that compilation is that the reported LODs cover a very wide range of concentrations, from 0.1 mM (ref. 91) to 8 zM,¹²⁴ which represents a remarkable spread of 16 orders of magnitude. In the following, we discuss the different factors that can influence the LOD in GFETs.

First, we note that methodologies to determine the LOD vary between studies. They can usually be classified in one of two categories: extrapolation^{53,134,189,190} or direct measurement,^{41,49,65,89,120,121,174} illustrated in Fig. 5b and c respectively. Both approaches first require precise characterization of the sensor baseline, *i.e.* the value and standard deviation of the chosen electrical metric (ex. CNP voltage, current) in absence of the targeted analyte. The LOD differs from the baseline of the sensor by an interval of confidence, defined as a chosen multiple of the standard deviation. The International Union of Pure and Applied Chemistry defines the LOD to be at three times the standard deviation,¹⁹¹ and the number of repli-

cas for baseline measurement is recommended at $n = 20$.¹⁹² In the first approach, the electrical metric is measured in presence of different concentrations of analyte, and the resulting response is extrapolated towards lower concentrations. The LOD is then identified as the concentration value at which the extrapolation function intersects with the upper bound of the interval of confidence. For example, Chen *et al.*⁵⁰ used a linear fit to extract a correlation between the relative current change observed in time series and the logarithm of analyte concentration. From data taken in a range of 10 nM to 100 μM , they extrapolated this linear fit until reaching a signal-to-noise ratio of 3, and obtained an LOD value of 0.3 nM. More complex non-linear fits can be used as well for extrapolation, such as a Hill-Langmuir equation as used by Li *et al.*³⁹ The second approach consists in actually making measurements at decreasing concentrations, with replicas, until the observed change in the electrical metric is no longer statistically different from the interval of confidence. For instance, Cai *et al.*⁴³ measured the sensor response for concentrations down to 10 fM of complementary DNA. However, after assessing the noise level with a blank control test, the LOD was established at 100 fM, corresponding to a signal exceeding three times the background level. This underlines the importance of assessing the baseline value and its variance. In some specific cases, it is more relevant to use another threshold than the baseline signal to determine the LOD. For example, in Campos *et al.*,⁸¹ the LOD of perfectly-matched DNA is determined as the concentration sharing the same signal value as the highest signal obtained with single-mismatched DNA. In general, the LOD assessment method should be detailed in order to enable proper benchmarking between studies. In our literature survey (see ESI†), the LOD values were taken as reported, without adjustment for the determination method. Extrapolation methods tend to require less measurements, but the extracted LOD can be off the mark if analyte signal deviates from the extrapolation model at low concentrations. In this case the second type of approach is the most reliable as it ensures that



Another class of negative controls is to test the sensors against the targeted analyte, but without the appropriate probe, to ensure that the response is due to analyte:probe binding and not to non-specific adsorption of the analyte on the sensor. Several groups have reported on the non-specific interaction of their targeted analyte with pristine graphene without probes.^{78,78,121,121,125} A limitation of such experiments is that non-specific interactions of the analyte with the sensor surface are likely to be very different between pristine and probe-functionalized graphene. A strategy to better simulate the actual sensor surface is to prepare sensors with alternative probes having no affinity for the targeted analyte.^{42,49,55} For instance, Lerner *et al.*⁴⁹ functionalized the surface of control sensors with scFv fragments of anti-HER2 antibodies, unspecific to the target nalodextrone, instead of the specific MUR μ -receptor. Similarly, Hajian *et al.*⁵⁵ prepared control sensors by loading a non-complementary single-guide RNA sequence in the dCas9 protein (instead of the complementary sequence). Such approaches enable control experiments with a sensor interface very similar to the regular experiment.

Positive controls are meant to validate that the sensor generates a signal if the analyte is present in the sample. The most common approach is to prepare calibration samples containing a known concentration of the targeted analyte. Most studies look for a dependence with analyte concentration to demonstrate that the measured signal is indeed due to the analyte. In such assays, target molecules are most commonly diluted in blank saline buffer,^{42,88,90,117} sometimes with a calibrated mix of interfering species.^{53,55,83,91,118} These calibration assays are usually presented as a proof of concept for the sensors, and they are sometimes used as positive controls before assays on cell culture samples,^{51,56} clinical samples^{55,115,121,136,198} or other environmental samples,^{46,123} in which the concentration is either unknown or measured with another detection technique to compare results. For instance, Wang *et al.*¹²¹ were the first group to measure the concentration of lead ions in real blood samples with GFET sensors, using a calibration with positive controls in buffer. GFETs results were found in good agreement with measurements by ICP-MS, confirming the potential of GFET technology for medical applications. For large analytes, some studies use imaging strategies to confirm by visualization the immobilization of the analyte on the GFET surface. As examples, Chen *et al.*⁷⁸ performed fluorescence microscopy, scanning electron microscopy (SEM), and atomic force microscopy (AFM) to visualize the capture of *E. coli* bacterial cells onto the surface of functionalized GFET devices, and Xu *et al.*¹⁵⁸ used DNA probes labelled with Cy3 or Cy5 fluorophores to correlate the electrical response of GFETs with fluorescence measurements.

4.4. Response time

An important practical aspect of sensor performance is the test duration, *i.e.* the time required to obtain the result of an analysis. For a given sensor technology, estimating this metric is critical to identify potential applications and to determine how

the sensors will be packaged, deployed and used. GFETs are often praised as fast detection tools,^{53,54,120,200} however there is often a lack of clarity as to which steps of their operating protocol are included in this assessment. Specifically, the process of analyte detection or quantitation using GFETs usually require several steps: sample injection, incubation, washing, all repeated for a number of replica and controls. The duration of each of these steps can be informed by real-time measurements with time series. In particular, the response time, *i.e.* the time required for the signal to stabilize after injection of the sample, or after its washing away, can be extracted from time series. Independently of analyte binding kinetics, part of the response time comes from the basal response of the sensor to perturbations in the medium when injecting/washing the sample or changing applied electric potentials. It is possible to assess this contribution to the response time by changing abruptly the gate voltage and measuring the response of electrical metrics in time series.⁶¹

Response times reported for GFETs in the literature vary significantly between experiments, even for similar analytes. For ions, response times are usually small, from almost instantaneous^{51,122,123} to approximately 100 seconds.³⁹ For proteins, there is a wider variability: for example, Lei *et al.*¹⁷⁴ recorded signal reaching a plateau 10 s after insertion of the analyte brain natriuretic peptide, whereas Kim *et al.*⁴¹ assessed a response time to the prostate antigen PSA of approximately 10 minutes. For DNA hybridization, most studies focus on quantitation experiments using before/after measurements. Incubation times between the two are typically long to maximize hybridization density: from 30 minutes^{65,161} to many hours.⁴⁴ Outside that range, Hajian *et al.*⁵⁵ reported a detection of 1.7 fM in 15 minutes, due to the dCas9 system which actively improves the processing of DNA strands in the sample. The experimental process used to determine these incubation times is seldom described and likely to be based on trial and error, although a few real-time experiments have looked specifically at hybridization and denaturation kinetics.^{53,57} Some groups notice a significant variation of the response time with target concentration,^{53,57} such as observed by Xu *et al.*⁵³ in Fig. 2h. Others define the response time as the time required to reach current saturation in all tested concentrations, in order to determine an incubation time independent of target concentrations.^{41,42} Finally, continuous flow settings appear a promising solution to minimize incubation times, as they report faster response times than standard configurations based on injection followed by static incubation periods. With a 30 $\mu\text{L min}^{-1}$ flow, Stine *et al.*¹³⁴ reported a saturation of signal in less than 800 seconds for the hybridization of fully complementary ssDNA targets at 1 μM concentration. Xu *et al.*⁵³ obtained a stabilized hybridization signal in less than a minute for the same target concentration at 60 $\mu\text{L min}^{-1}$ flow.

4.5. Other considerations

Depending on which applications are targeted for the GFET biosensors, numerous practical issues are important to con-



sider in assessing their suitability and potential performance. Here, we merely raise some of the considerations that have been explored in the development of GFET sensor technology. Scalable production is an important aspect towards commercialization, in order to achieve competitive production rates and costs: scalable processes for GFET assembly have been developed, usually based on CVD synthesis techniques.^{65,201} Reusability, *i.e.* the possibility to make successive analyses on the same device, as well as shelf-life of the sensors are other important parameters in technology maturation, and have been tested in some recent studies. For example, reusability has been tested by Wu *et al.*¹⁹⁸ by performing successive binding–unbinding cycles with the target and measuring the evolution in the strength of signal, finding a conservation of signal of 94% when comparing the first to the last cycle. Some groups also made assessments of shelf-life by measuring the drift of current over time for multiple concentrations of target¹¹⁹ or by repeating experiments after storage time.⁶⁴ Reported shelf-life values vary from one week⁴⁹ to a few months.^{119,156} The use of flexible substrates is also an ongoing area of investigation for wearable or skin-implanted devices, for example to detect glucose levels in sweat directly on the skin¹⁵⁹ or for other health-monitoring purposes.²⁰² Silk fibroin,⁹¹ paper substrates^{92,202} or polyimide¹⁵⁹ have been successfully tested as flexible substrates.

5. Conclusions

Graphene field-effect transistors have demonstrated promising performance as bioanalytical sensors, including low limits of detection and fast response times in a miniature footprint. Their core feature is the use of graphene conductance as transducer, which provides high sensitivity to the capture of biomolecular species at its surface due to its monoatomic thinness. For the past decade, GFET sensors have been prototyped for a wide variety of biologically-relevant analytes: ions, small molecules, nucleic acids and proteins. We reviewed this literature (see ESI†) to discuss best practices in sensor assembly, experimental design and performance assessment, in particular towards the detection, quantitation and kinetic analysis of biomolecules. In sensor design, the type of graphene (exfoliation, CVD, rGO) does not appear as a dominant factor for performance: very low LODs have been reported for high- and low-quality graphene. Two more critical features are the configuration of the gate electrode and the assembly of the biorecognition interface: both would benefit from better modeling of their effect on graphene conductance transduction. In particular, the specifics of the surface chemistry (*e.g.* coverage, orientation, stability of immobilized probes, blocking species and captures analytes, and their respective interactions) are often not well known or controlled. On the other hand, limitations due to media screening appear well-understood and modeled by the Debye length, and strategies have been successfully proposed to increase the range of detection. The transduction of

analyte capture in electrical conductance can appear as a change in the density of charge carriers by doping (*i.e.* shift of the charge neutrality point), in the scattering processes (*i.e.* change in the transconductance), or a combination of them. Transfer curves, alone or combined with time series, are the most appropriate way of studying the physics of this interaction. Some interrogations remain about the coupling mechanism between analyte capture and graphene, as shown by the diverging CNP shift polarities reported for similar analytes. Time series of electrical current alone are not sufficient to interpret interactions mechanisms, but they can provide a robust empirical assessment of target presence or quantification, and they are essential for kinetic studies. Two-dimensional time series combining gate voltage and time sweeps provide both mechanistic and kinetic information in the same measurement. In all cases, in order to produce a reliable and reproducible experiment, intra- and inter-device variabilities need to be assessed and managed using sufficient replicas and appropriate controls. Finally, scalability and cost of fabrication, electronics and fluidics packaging for practical use with samples, as well as reproducibility and stability of the sensor response are important aspects to optimize in order to move the technology forward.

Conflicts of interest

There are no conflicts to declare.

Acknowledgements

The authors acknowledge financial support from the Canada Research Chairs, Canada's Natural Science and Engineering Council (NSERC) and New Frontier Research Fund – Exploration, Fonds de recherche du Québec - Nature et Technologie (FRQNT), and the Institute for Research in Immunology and Cancer (IRIC) of Université de Montréal. A. Béraud and A. Bencherif acknowledge scholarships from IRIC, and M. Sauvage from the TransMedTech Institute. The authors also thank Richard Martel (U. Montréal) for generous support.

References

- 1 Z. Shabaninejad, F. Yousefi, A. Movahedpour, Y. Ghasemi, S. Dokanehiifard, S. Rezaei, R. Aryan, A. Savardashtaki and H. Mirzaei, *Anal. Biochem.*, 2019, **581**, 113349.
- 2 G. Reina, J. M. González-Domínguez, A. Criado, E. Vázquez, A. Bianco and M. Prato, *Chem. Soc. Rev.*, 2017, **46**, 4400–4416.
- 3 T. Saliev, *C*, 2019, **5**, 29.
- 4 A. Zubiarrain-Laserna and P. Kruse, *J. Electrochem. Soc.*, 2020, **167**, 037539.
- 5 K. R. Rogers, *Biosens. Bioelectron.*, 1995, **10**, 533–541.
- 6 S. Xu, *Microchim. Acta*, 2012, **178**, 245–260.



- 7 A. M. Vaidya and U. S. Annapure, *Enzymes in Food Biotechnology*, Academic Press, 2019, pp. 659–674.
- 8 C. Kokkinos, *Nanomaterials*, 2019, **9**, 1361.
- 9 K. E. Sapsford, T. Pons, I. L. Medintz and H. Mattoussi, *Sensors*, 2006, **6**, 925–953.
- 10 Y. Feng, Y. Zhang, C. Ying, D. Wang and C. Du, *Genomics, Proteomics Bioinf.*, 2015, **13**, 4–16.
- 11 Z. Li, W. Zhang and F. Xing, *Int. J. Mol. Sci.*, 2019, **20**, 2461.
- 12 S. Kruss, A. J. Hilmer, J. Zhang, N. F. Reuel, B. Mu and M. S. Strano, *Adv. Drug Delivery Rev.*, 2013, **65**, 1933–1950.
- 13 C.-M. Tilmaciu and M. C. Morris, *Front. Chem.*, 2015, **3**, 59.
- 14 M. Coroş, S. Pruneanu and R.-I. S.-v. Staden, *J. Electrochem. Soc.*, 2019, **167**, 037528.
- 15 X. Zang, Q. Zhou, J. Chang, Y. Liu and L. Lin, *Microelectron. Eng.*, 2015, **132**, 192–206.
- 16 M. J. Schöning and A. Poghossian, *Analyst*, 2002, **127**, 1137–1151.
- 17 S. Caras and J. Janata, *Anal. Chem.*, 1980, **52**, 1935–1937.
- 18 S. Mao, J. Chang, H. Pu, G. Lu, Q. He, H. Zhang and J. Chen, *Chem. Soc. Rev.*, 2017, **46**, 6872–6904.
- 19 A. Noy, A. B. Artyukhin and N. Misra, *Mater. Today*, 2009, **12**, 22–31.
- 20 L. Mu, Y. Chang, S. D. Sawtelle, M. Wipf, X. Duan and M. A. Reed, *IEEE Access*, 2015, **3**, 287–302.
- 21 B. L. Allen, P. D. Kichambare and A. Star, *Adv. Mater.*, 2007, **19**, 1439–1451.
- 22 G. Hou, L. Zhang, V. Ng, Z. Wu and M. Schulz, *Nano LIFE*, 2016, **06**, 1642006.
- 23 J. Wang, F. Shen, Z. Wang, G. He, J. Qin, N. Cheng, M. Yao, L. Li and X. Guo, *Angew. Chem., Int. Ed.*, 2014, **53**, 5038–5043.
- 24 Y. Choi, I. S. Moody, P. C. Sims, S. R. Hunt, B. L. Corso, I. Perez, G. A. Weiss and P. G. Collins, *Science*, 2012, **335**, 319–324.
- 25 D. Bouilly, J. Hon, N. S. Daly, S. Trocchia, S. Vernick, J. Yu, S. Warren, Y. Wu, R. L. Gonzalez, K. L. Shepard and C. Nuckolls, *Nano Lett.*, 2016, **16**, 4679–4685.
- 26 S. Das, J. A. Robinson, M. Dubey, H. Terrones and M. Terrones, *Annu. Rev. Mater. Res.*, 2015, **45**, 1–27.
- 27 D. L. Duong, S. J. Yun and Y. H. Lee, *ACS Nano*, 2017, **11**, 11803–11830.
- 28 K. S. Novoselov, A. K. Geim, S. V. Morozov, D. Jiang, Y. Zhang, S. V. Dubonos, I. V. Grigorieva and A. A. Firsov, *Science*, 2004, **306**, 666–669.
- 29 Y. Zhong, Z. Zhen and H. Zhu, *FlatChem*, 2017, **4**, 20–32.
- 30 M. A. Brown, M. S. Crosser, M. R. Leyden, Y. Qi and E. D. Minot, *Appl. Phys. Lett.*, 2016, **109**, 093104.
- 31 X.-M. Huang, L.-Z. Liu, S. Zhou and J.-J. Zhao, *Front. Phys.*, 2020, **15**, 33301.
- 32 B. Zhan, C. Li, J. Yang, G. Jenkins, W. Huang and X. Dong, *Small*, 2014, **10**, 4042–4065.
- 33 F. Schedin, A. K. Geim, S. V. Morozov, E. W. Hill, P. Blake, M. I. Katsnelson and K. S. Novoselov, *Nat. Mater.*, 2007, **6**, 652–655.
- 34 S. Mao, G. Lu and J. Chen, *J. Mater. Chem. A*, 2014, **2**, 5573–5579.
- 35 I. Fakih, F. Mahvash, M. Siaj and T. Szkopek, *Phys. Rev. Appl.*, 2017, **8**, 044022.
- 36 Y. Zhu, C. Wang, N. Petrone, J. Yu, C. Nuckolls, J. Hone and Q. Lin, *Appl. Phys. Lett.*, 2015, **106**, 123503.
- 37 N. Mohanty and V. Berry, *Nano Lett.*, 2008, **8**, 4469–4476.
- 38 H. G. Sudibya, Q. He, H. Zhang and P. Chen, *ACS Nano*, 2011, **5**, 1990–1994.
- 39 Y. Li, C. Wang, Y. Zhu, X. Zhou, Y. Xiang, M. He and S. Zeng, *Biosens. Bioelectron.*, 2017, **89**, 758–763.
- 40 Y. Zhu, Y. Hao, E. A. Adogla, J. Yan, D. Li, K. Xu, Q. Wang, J. Hone and Q. Lin, *Nanoscale*, 2016, **8**, 5815–5819.
- 41 D.-J. Kim, I. Y. Sohn, J.-H. Jung, O. J. Yoon, N. E. Lee and J.-S. Park, *Biosens. Bioelectron.*, 2013, **41**, 621–626.
- 42 D. Kwong Hong Tsang, T. J. Lieberthal, C. Watts, I. E. Dunlop, S. Ramadan, A. E. del Rio Hernandez and N. Klein, *Sci. Rep.*, 2019, **9**, 1–10.
- 43 B. Cai, S. Wang, L. Huang, Y. Ning, Z. Zhang and G.-J. Zhang, *ACS Nano*, 2014, **8**, 2632–2638.
- 44 M. T. Hwang, P. B. Landon, J. Lee, D. Choi, A. H. Mo, G. Glinsky and R. Lal, *Proc. Natl. Acad. Sci. U. S. A.*, 2016, **113**, 7088–7093.
- 45 Y. Huang, X. Dong, Y. Liu, L.-J. Li and P. Chen, *J. Mater. Chem.*, 2011, **21**, 12358–12362.
- 46 B. Thakur, G. Zhou, J. Chang, H. Pu, B. Jin, X. Sui, X. Yuan, C.-H. Yang, M. Magruder and J. Chen, *Biosens. Bioelectron.*, 2018, **110**, 16–22.
- 47 F. Liu, Y. H. Kim, D. S. Cheon and T. S. Seo, *Sens. Actuators, B*, 2013, **186**, 252–257.
- 48 J. W. Kim, S. Kim, Y.-h. Jang, K.-i. Lim and W. H. Lee, *Nanotechnology*, 2019, **30**, 345502.
- 49 M. B. Lerner, F. Matsunaga, G. H. Han, S. J. Hong, J. Xi, A. Crook, J. M. Perez-Aguilar, Y. W. Park, J. G. Saven, R. Liu and A. T. C. Johnson, *Nano Lett.*, 2014, **14**, 2709–2714.
- 50 X. Chen, Y. Liu, X. Fang, Z. Li, H. Pu, J. Chang, J. Chen and S. Mao, *Biosens. Bioelectron.*, 2019, **126**, 664–671.
- 51 S. Jiang, R. Cheng, X. Wang, T. Xue, Y. Liu, A. Nel, Y. Huang and X. Duan, *Nat. Commun.*, 2013, **4**, 1–7.
- 52 Z. Wang, K. Yi, Q. Lin, L. Yang, X. Chen, H. Chen, Y. Liu and D. Wei, *Nat. Commun.*, 2019, **10**, 1544.
- 53 S. Xu, J. Zhan, B. Man, S. Jiang, W. Yue, S. Gao, C. Guo, H. Liu, Z. Li, J. Wang and Y. Zhou, *Nat. Commun.*, 2017, **8**, 1–10.
- 54 L. Zuccaro, C. Tesauero, T. Kurkina, P. Fiorani, H. K. Yu, B. R. Knudsen, K. Kern, A. Desideri and K. Balasubramanian, *ACS Nano*, 2015, **9**, 11166–11176.
- 55 R. Hajian, S. Balderston, T. Tran, T. deBoer, J. Etienne, M. Sandhu, N. A. Wauford, J.-Y. Chung, J. Nokes, M. Athaiya, J. Paredes, R. Peytavi, B. Goldsmith, N. Murthy, I. M. Conboy and K. Aran, *Nat. Biomed. Eng.*, 2019, **3**, 427–437.
- 56 S. Islam, S. Shukla, V. K. Bajpai, Y.-K. Han, Y. S. Huh, A. Ghosh and S. Gandhi, *Sci. Rep.*, 2019, **9**, 1–7.
- 57 Z. Gao, H. Xia, J. Zauberman, M. Tomaiuolo, J. Ping, Q. Zhang, P. Ducos, H. Ye, S. Wang, X. Yang, F. Lubna,



- Z. Luo, L. Ren and A. T. C. Johnson, *Nano Lett.*, 2018, **18**, 3509–3515.
- 58 R. Vishnubhotla, A. Sriram, O. O. Dickens, S. V. Mandyam, J. Ping, E. Adu-Beng and A. C. Johnson, *IEEE Sens. J.*, 2020, 1–1.
- 59 M. T. Hwang, M. Heiranian, Y. Kim, S. You, J. Leem, A. Taqieddin, V. Faramarzi, Y. Jing, I. Park, A. M. van der Zande, S. Nam, N. R. Aluru and R. Bashir, *Nat. Commun.*, 2020, **11**, 1543.
- 60 C. Chan, J. Shi, Y. Fan and M. Yang, *Sens. Actuators, B*, 2017, **251**, 927–933.
- 61 X. Wang, Z. Hao, T. R. Olsen, W. Zhang and Q. Lin, *Nanoscale*, 2019, **11**, 12573–12581.
- 62 N. I. Khan, M. Mousazadehkasin, S. Ghosh, J. G. Tsavalas and E. Song, *Analyst*, 2020, **145**, 4494–4503.
- 63 G. Xu, J. Abbott, L. Qin, K. Y. M. Yeung, Y. Song, H. Yoon, J. Kong and D. Ham, *Nat. Commun.*, 2014, **5**, 1–9.
- 64 G. Saltzgaber, P. M. Wojcik, T. Sharf, M. R. Leyden, J. L. Wardini, C. A. Heist, A. A. Adenuga, V. T. Remcho and E. D. Minot, *Nanotechnology*, 2013, **24**, 355502.
- 65 J. Ping, R. Vishnubhotla, A. Vrudhula and A. T. C. Johnson, *ACS Nano*, 2016, **10**, 8700–8704.
- 66 W. Fu, L. Jiang, E. P. v. Geest, L. M. C. Lima and G. F. Schneider, *Adv. Mater.*, 2017, **29**, 1603610.
- 67 R. Forsyth, A. Devadoss and O. J. Guy, *Diagnostics*, 2017, **7**, 45.
- 68 T. Terse-Thakoor, S. Badhulika and A. Mulchandani, *J. Mater. Res.*, 2017, **32**, 2905–2929.
- 69 S. Szunerits and R. Boukherroub, *Interface Focus*, 2018, **8**, 20160132.
- 70 X. Wu, F. Mu, Y. Wang and H. Zhao, *Molecules*, 2018, **23**, 2050.
- 71 L. Xu, Y. Wen, S. Pandit, V. R. S. S. Mokkapatil, I. Mijakovic, Y. Li, M. Ding, S. Ren, W. Li and G. Liu, *BMC Chem.*, 2019, **13**, 112.
- 72 P. Salvo, B. Melai, N. Calisi, C. Paoletti, F. Bellagambi, A. Kirchhain, M. G. Trivella, R. Fuoco and F. Di Francesco, *Sens. Actuators, B*, 2018, **256**, 976–991.
- 73 D. G. Papageorgiou, I. A. Kinloch and R. J. Young, *Prog. Mater. Sci.*, 2017, **90**, 75–127.
- 74 F. Bonaccorso, Z. Sun, T. Hasan and A. C. Ferrari, *Nat. Photonics*, 2010, **4**, 611–622.
- 75 A. K. Geim and K. S. Novoselov, *Nat. Mater.*, 2007, **6**, 183–191.
- 76 P. Kumar Srivastava and S. Ghosh, *Appl. Phys. Lett.*, 2013, **102**, 043102.
- 77 M. Yi and Z. Shen, *J. Mater. Chem. A*, 2015, **3**, 11700–11715.
- 78 Y. Chen, Z. P. Michael, G. P. Kotchey, Y. Zhao and A. Star, *ACS Appl. Mater. Interfaces*, 2014, **6**, 3805–3810.
- 79 X. Chen, L. Zhang and S. Chen, *Synth. Met.*, 2015, **210**, 95–108.
- 80 W. A. d. Heer, C. Berger, M. Ruan, M. Sprinkle, X. Li, Y. Hu, B. Zhang, J. Hankinson and E. Conrad, *Proc. Natl. Acad. Sci. U. S. A.*, 2011, **108**, 16900–16905.
- 81 R. Campos, J. Borme, J. R. Guerreiro, G. Machado, M. F. Cerqueira, D. Y. Petrovykh and P. Alpuim, *ACS Sens.*, 2019, **4**, 286–293.
- 82 B. Chen, H. Huang, X. Ma, L. Huang, Z. Zhang and L.-M. Peng, *Nanoscale*, 2014, **6**, 15255–15261.
- 83 S. Xu, S. Jiang, C. Zhang, W. Yue, Y. Zou, G. Wang, H. Liu, X. Zhang, M. Li, Z. Zhu and J. Wang, *Appl. Surf. Sci.*, 2018, **427**, 1114–1119.
- 84 J. Chang, S. Mao, Y. Zhang, S. Cui, G. Zhou, X. Wu, C.-H. Yang and J. Chen, *Nanoscale*, 2013, **5**, 3620–3626.
- 85 M. Wojtoniszak, X. Chen, R. J. Kalenczuk, A. Wajda, J. Łapczuk, M. Kurzewski, M. Drozdziak, P. K. Chu and E. Borowiak-Palen, *Colloids Surf., B*, 2012, **89**, 79–85.
- 86 R. Negishi and Y. Kobayashi, *Appl. Phys. Lett.*, 2014, **105**, 253502.
- 87 P. Li, B. Liu, D. Zhang, Y. Sun and J. Liu, *Appl. Phys. Lett.*, 2016, **109**, 153101.
- 88 S. Okamoto, Y. Ohno, K. Maehashi, K. Inoue and K. Matsumoto, *Jpn. J. Appl. Phys.*, 2012, **51**, 06FD08.
- 89 K. Islam, A. Suhail and G. Pan, *Biosensors*, 2017, **7**, 27.
- 90 T. Ono, Y. Kanai, K. Inoue, Y. Watanabe, S.-i. Nakakita, T. Kawahara, Y. Suzuki and K. Matsumoto, *Nano Lett.*, 2019, **19**, 4004–4009.
- 91 X. You and J. J. Pak, *Sens. Actuators, B*, 2014, **202**, 1357–1365.
- 92 A. A. Cagang, I. H. Abidi, A. Tyagi, J. Hu, F. Xu, T. J. Lu and Z. Luo, *Anal. Chim. Acta*, 2016, **917**, 101–106.
- 93 Y. Huang, E. Sutter, N. N. Shi, J. Zheng, T. Yang, D. Englund, H.-J. Gao and P. Sutter, *ACS Nano*, 2015, **9**, 10612–10620.
- 94 Y. Chen, X.-L. Gong and J.-G. Gai, *Adv. Sci.*, 2016, **3**, 1500343.
- 95 L. Gao, W. Ren, H. Xu, L. Jin, Z. Wang, T. Ma, L.-P. Ma, Z. Zhang, Q. Fu, L.-M. Peng, X. Bao and H.-M. Cheng, *Nat. Commun.*, 2012, **3**, 1–7.
- 96 C. T. Cherian, F. Giustiniano, I. Martin-Fernandez, H. Andersen, J. Balakrishnan and B. Özyilmaz, *Small*, 2015, **11**, 189–194.
- 97 J. W. Suk, A. Kitt, C. W. Magnuson, Y. Hao, S. Ahmed, J. An, A. K. Swan, B. B. Goldberg and R. S. Ruoff, *ACS Nano*, 2011, **5**, 6916–6924.
- 98 X. Wang, L. Zhi and K. Müllen, *Nano Lett.*, 2008, **8**, 323–327.
- 99 G. Eda, G. Fanchini and M. Chhowalla, *Nat. Nanotechnol.*, 2008, **3**, 270–274.
- 100 S. Wang, M. Z. Hossain, K. Shinozuka, N. Shimizu, S. Kitada, T. Suzuki, R. Ichige, A. Kuwana and H. Kobayashi, *Biosens. Bioelectron.*, 2020, **165**, 112363.
- 101 K. Maehashi, Y. Sofue, S. Okamoto, Y. Ohno, K. Inoue and K. Matsumoto, *Sens. Actuators, B*, 2013, **187**, 45–49.
- 102 S. Farid, X. Meshik, M. Choi, S. Mukherjee, Y. Lan, D. Parikh, S. Poduri, U. Batteredene, C.-E. Huang, Y. Y. Wang, P. Burke, M. Dutta and M. A. Stroschio, *Biosens. Bioelectron.*, 2015, **71**, 294–299.
- 103 E. D. Minot, A. M. Janssens, I. Heller, H. A. Heering, C. Dekker and S. G. Lemay, *Appl. Phys. Lett.*, 2007, **91**, 093507.
- 104 T.-Y. Chen, P. T. K. Loan, C.-L. Hsu, Y.-H. Lee, J. T.-W. Wang, K.-H. Wei, C.-T. Lin and L.-J. Li, *Biosens. Bioelectron.*, 2013, **41**, 103–109.



- 152 J. C. Genereux and J. K. Barton, *Chem. Rev.*, 2010, **110**, 1642–1662.
- 153 J. G. Champlain, *J. Appl. Phys.*, 2011, **109**, 084515.
- 154 J. H. Chen, C. Jang, M. Ishigami, S. Xiao, W. G. Cullen, E. D. Williams and M. S. Fuhrer, *Solid State Commun.*, 2009, **149**, 1080–1086.
- 155 E. Akbari, N. Nabipour, S. M. Hadavi and M. Nilashi, *J. Mater. Sci.: Mater. Electron.*, 2020, 6461–6466.
- 156 H. Li, Y. Zhu, M. Islam, M. Rahman, K. Walsh and G. Koley, *Sens. Actuators, B*, 2017, **253**, 759–765.
- 157 Q. Yuan, S. Wu, C. Ye, X. Liu, J. Gao, N. Cui, P. Guo, G. Lai, Q. Wei, M. Yang, W. Su, H. Li, N. Jiang, L. Fu, D. Dai, C.-T. Lin and K. W. A. Chee, *Sens. Actuators, B*, 2019, **285**, 333–340.
- 158 K. Xu, X. Meshik, B. M. Nichols, E. Zakar, M. Dutta and M. A. Stroschio, *Nanotechnology*, 2014, **25**, 205501.
- 159 C. Huang, Z. Hao, T. Qi, Y. Pan and X. Zhao, *J. Materiomics*, 2020, 308–314.
- 160 A. K. Manoharan, S. Chinnathambi, R. Jayavel and N. Hanagata, *Sci. Technol. Adv. Mater.*, 2017, **18**, 43–50.
- 161 B. Cai, L. Huang, H. Zhang, Z. Sun, Z. Zhang and G.-J. Zhang, *Biosens. Bioelectron.*, 2015, **74**, 329–334.
- 162 S. Chen, Y. Sun, Y. Xia, K. Lv, B. Man and C. Yang, *Biosens. Bioelectron.*, 2020, **156**, 112128.
- 163 S. Gowtham, R. H. Scheicher, R. Ahuja, R. Pandey and S. P. Karna, *Phys. Rev. B: Condens. Matter Mater. Phys.*, 2007, **76**, 033401.
- 164 J. Antony and S. Grimme, *Phys. Chem. Chem. Phys.*, 2008, **10**, 2722–2729.
- 165 C.-T. Lin, P. T. K. Loan, T.-Y. Chen, K.-K. Liu, C.-H. Chen, K.-H. Wei and L.-J. Li, *Adv. Funct. Mater.*, 2013, **23**, 2301–2307.
- 166 J. Lin, D. Teweldebrhan, K. Ashraf, G. Liu, X. Jing, Z. Yan, R. Li, M. Ozkan, R. K. Lake, A. A. Balandin and C. S. Ozkan, *Small*, 2010, **6**, 1150–1155.
- 167 A. Kokil, K. Yang and J. Kumar, *J. Polym. Sci., Part B: Polym. Phys.*, 2012, **50**, 1130–1144.
- 168 X. Liang, Z. Fu and S. Y. Chou, *Nano Lett.*, 2007, **7**, 3840–3844.
- 169 K. I. Bolotin, K. J. Sikes, Z. Jiang, M. Klima, G. Fudenberg, J. Hone, P. Kim and H. L. Stormer, *Solid State Commun.*, 2008, **146**, 351–355.
- 170 M. Larisika, C. Kotlowski, C. Steininger, R. Mastrogiacomio, P. Pelosi, S. Schütz, S. F. Peteu, C. Kleber, C. Reiner-Rozman, C. Nowak and W. Knoll, *Angew. Chem., Int. Ed.*, 2015, **54**, 13245–13248.
- 171 J. S. Moon, M. Antcliffe, H. C. Seo, D. Curtis, S. Lin, A. Schmitz, I. Milosavljevic, A. A. Kiselev, R. S. Ross, D. K. Gaskill, P. M. Campbell, R. C. Fitch, K.-M. Lee and P. Asbeck, *Appl. Phys. Lett.*, 2012, **100**, 203512.
- 172 N. Vandecasteele, A. Barreiro, M. Lazzeri, A. Bachtold and F. Mauri, *Phys. Rev. B: Condens. Matter Mater. Phys.*, 2010, **82**, 045416.
- 173 T. Cohen-Karni, Q. Qing, Q. Li, Y. Fang and C. M. Lieber, *Nano Lett.*, 2010, **10**, 1098–1102.
- 174 Y.-M. Lei, M.-M. Xiao, Y.-T. Li, L. Xu, H. Zhang, Z.-Y. Zhang and G.-J. Zhang, *Biosens. Bioelectron.*, 2017, **91**, 1–7.
- 175 R. C. Fries, *Reliable Design of Medical Devices*, CRC Press, 2016.
- 176 E. Stern, R. Wagner, F. J. Sigworth, R. Breaker, T. M. Fahmy and M. A. Reed, *Nano Lett.*, 2007, **7**, 3405–3409.
- 177 N. S. Green and M. L. Norton, *Anal. Chim. Acta*, 2015, **853**, 127–142.
- 178 S. Sorgenfrei, C.-y. Chiu, M. Johnston, C. Nuckolls and K. L. Shepard, *Nano Lett.*, 2011, **11**, 3739–3743.
- 179 G.-J. Zhang, G. Zhang, J. H. Chua, R.-E. Chee, E. H. Wong, A. Agarwal, K. D. Buddharaju, N. Singh, Z. Gao and N. Balasubramanian, *Nano Lett.*, 2008, **8**, 1066–1070.
- 180 A. Vacic, J. M. Criscione, N. K. Rajan, E. Stern, T. M. Fahmy and M. A. Reed, *J. Am. Chem. Soc.*, 2011, **133**, 13886–13889.
- 181 L. Kergoat, B. Piro, M. Berggren, M.-C. Pham, A. Yassar and G. Horowitz, *Org. Electron.*, 2012, **13**, 1–6.
- 182 K. Matsumoto, K. Maehashi, Y. Ohno and K. Inoue, *J. Phys. D: Appl. Phys.*, 2014, **47**, 094005.
- 183 Y. Ohno, K. Maehashi and K. Matsumoto, *J. Am. Chem. Soc.*, 2010, **132**, 18012–18013.
- 184 O. S. Kwon, S. J. Park, J.-Y. Hong, A.-R. Han, J. S. Lee, J. S. Lee, J. H. Oh and J. Jang, *ACS Nano*, 2012, **6**, 1486–1493.
- 185 N. Gao, W. Zhou, X. Jiang, G. Hong, T.-M. Fu and C. M. Lieber, *Nano Lett.*, 2015, **15**, 2143–2148.
- 186 G. Palazzo, D. D. Tullio, M. Magliulo, A. Mallardi, F. Intranuovo, M. Y. Mulla, P. Favia, I. Vikholm-Lundin and L. Torsi, *Adv. Mater.*, 2015, **27**, 911–916.
- 187 J. D. Ingle, *J. Chem. Educ.*, 1974, **51**, 100.
- 188 A. A. Balandin, *Nat. Nanotechnol.*, 2013, **8**, 549–555.
- 189 Z. Hao, Y. Zhu, X. Wang, P. G. Rotti, C. DiMarco, S. R. Tyler, X. Zhao, J. F. Engelhardt, J. Hone and Q. Lin, *ACS Appl. Mater. Interfaces*, 2017, **9**, 27504–27511.
- 190 N. M. Andoy, M. S. Filipiak, D. Vetter, S. Gutiérrez-Sanz and A. Tarasov, *Adv. Mater. Technol.*, 2018, **3**, 1800186.
- 191 L. A. Currie, *Pure Appl. Chem.*, 1995, **67**, 1699–1723.
- 192 D. A. Armbruster and T. Pry, *Clin. Biochem. Rev.*, 2008, **29**, S49–S52.
- 193 F. Yu, D. Yao and W. Knoll, *Nucleic Acids Res.*, 2004, **32**, e75.
- 194 T. R. Hughes, M. Mao, A. R. Jones, J. Burchard, M. J. Marton, K. W. Shannon, S. M. Lefkowitz, M. Ziman, J. M. Schelter, M. R. Meyer, S. Kobayashi, C. Davis, H. Dai, Y. D. He, S. B. Stephaniants, G. Cavet, W. L. Walker, A. West, E. Coffey, D. D. Shoemaker, R. Stoughton, A. P. Blanchard, S. H. Friend and P. S. Linsley, *Nat. Biotechnol.*, 2001, **19**, 342–347.
- 195 Y. Ohno, K. Maehashi, Y. Yamashiro and K. Matsumoto, *Nano Lett.*, 2009, **9**, 3318–3322.
- 196 M. Hasegawa, Y. Hirayama, Y. Ohno, K. Maehashi and K. Matsumoto, *Jpn. J. Appl. Phys.*, 2014, **53**, 05FD05.
- 197 F. Schwierz, *Nat. Nanotechnol.*, 2010, **5**, 487–496.
- 198 D. Wu, Y. Yu, D. Jin, M.-M. Xiao, Z.-Y. Zhang and G.-J. Zhang, *Anal. Chem.*, 2020, **92**, 4006–4015.



- 199 E. Pembroke, G. Ruan, A. Sinitskii, D. A. Corley, Z. Yan, Z. Sun and J. M. Tour, *Nano Res.*, 2013, **6**, 138–148.
- 200 S. Mao, H. Pu, J. Chang, X. Sui, G. Zhou, R. Ren, Y. Chen and J. Chen, *Environ. Sci.: Nano*, 2017, **4**, 856–863.
- 201 M. B. Lerner, J. Dailey, B. R. Goldsmith, D. Brisson and A. T. Charlie Johnson, *Biosens. Bioelectron.*, 2013, **45**, 163–167.
- 202 K. Bhatt, S. Kumar and C. C. Tripathi, *Pramana – J. Phys.*, 2020, **94**, 31.

